PAPER

Check for updates

Synthesis of chiral mesoporous silica nanoparticles for the adsorptive removal of the chiral insecticide sulfoxaflor from water

Sarah Alharthi, [ID] [ab] Ashraf Ali [ID] *[ce] and Eman Y. Santali[d]

Mesoporous materials have garnered significant interest because of their porous structure, large surface area and ease of surface functionalization to incorporate the functional groups of choice. Herein, chiral mesoporous silica nanoparticles (CMSNPs) were prepared using quaternary amino silane as the template, tetramethyl orthosilicate as the silica source and proline and cellulose as chiral selector. The developed CMSNPs were characterized by scanning electron microscopy (SEM), transmission electron microscopy (TEM), elemental analysis, Fourier transform infrared (FTIR) spectroscopy, X-ray diffraction analysis, BET surface area analysis and BJH pore size/volume analysis. It was observed that the CMSNPs have high specific surface area and narrow particle size and pore size distribution. These CMSNPs were used as adsorbents for separation of the chiral insecticide sulfoxaflor. The effects of various parameters that affect adsorption, such as initial concentration of the analyte, adsorbent dose, time and pH, were evaluated, and the optimum values were determined. At optimum conditions, the removal efficiency and adsorption capacity were 98.5% and 435.45 mg g^{-1}, respectively. Further, adsorption isothermal study was carried out using Freundlich and Langmuir models. Results showed that mesoporous silica nanoparticles functionalized with amide-bonded cellulose are promising and cost-effective adsorbents for the removal of chiral pesticides from water and wastewater.

1. Introduction

The global need for increased food production has resulted in excessive use of pesticides and fertilizers, which have caused serious environmental effects and raised public health concerns.[1,2] Traces of pesticides have been detected in surface and groundwater, which are the major sources of drinking water.[3] The presence of various pesticides and their derivatives in water and soil is particularly concerning as pesticides are harmful even at very low concentrations (pg L^{-1} to ng L^{-1}).[4] Industries and agriculture sector are the major sources of releasing pesticides into the environment.[1] Wastewater from pesticide-producing industries contaminates water bodies, which in turn affects humans and other living organisms when they consume food and water contaminated with pesticides. The most widely used pesticides are organophosphates, carbamates, pyrethroids and organochlorines. Different pesticides have different toxicity levels depending on their chemical composition and mode of action and the toxicity of pesticides could be acute or chronic. Acute toxicity results from short term exposure, while chronic toxicity results from long term exposure to the chemical. In acute toxicity, harmful effects are due to a single exposure by any means, such as *via* ingestion, skin contact or inhalation and causes headache, nausea, dizziness, stress, *etc.* In contrast, tumors, birth defects, genetic disorders, nervous and reproductive disorders are the results of chronic toxicity. Therefore, it is necessary to efficiently remove pesticides from water, soil and food samples.[5]

About thirty percent of currently registered pesticides exhibit chirality, and they typically show some degree of stereoselectivity that affects their toxicity and/or biodegradation rates.[3,4] Given that the vast majority of chiral pesticides are produced and used as racemic mixtures, it is necessary to determine their stereoselectivity in order to enhance risk assessment and provide an explanation for the creation of single- or enriched-enantiomer products.[6,7] Sulfoxaflor[methyl(oxo),1-[6-(trifluoromethyl)-3-pyridyl]ethyl-λ6-sulfanylidene] cyanamide was the first compound that was chosen for commercial development.[8] Compared to other insecticides, members of this class have a distinct set of structure–activity relationships (SAR) because of the presence of sulfoximine, which is a unique chemical moiety and the first of its kind in

[a]Department of Chemistry, College of Science, Taif University, Taif 21944, Saudi Arabia

[b]Research Center of Basic Sciences, Engineering and High Altitude, Taif University, Taif 21944, Saudi Arabia

[c]Department of Chemistry, Faculty of Physical & Applied Sciences, The University of Haripur, Haripur 22620, Pakistan. E-mail: ashrafaliswati@gmail.com

[d]Department of Pharmaceutical Chemistry, College of Pharmacy, Taif University, Taif, 21944, Saudi Arabia

[e]School of Chemistry & Chemical Engineering, Henan University of Technology, Zhengzhou 450000, China

a commercial pesticide. Sulfoximines are effective in controlling a wide variety of sap-feeding insects/pests, including those that are resistant to neonicotinoids.[9]

Various methods, such as membrane separation, ozonation, solvent extraction, oxidation, and chlorination, are used for the removal of pesticides. These techniques have several drawbacks, including the production of secondary waste, high operating costs, and inefficient removal. Therefore, to eliminate pesticides from water samples, more effective, fast, and reliable remediation techniques are needed. Adsorption is an attractive alternative method for pesticide removal because of its simple design, high removal efficiency, and low costs of operation.[10,11] Various adsorbents, such as activated carbon,[12] metal organic frameworks,[13] agricultural by-products,[14] clay minerals,[15] zeolites,[16] biosorbents[17] and mesoporous silica-based adsorbents,[18,19] have been reported for the removal of pesticides.

Mesoporous silica and silica-based materials have garnered a lot of interest because of their large surface area, ordered pore distribution, narrow particle size distribution, high thermal stability, and ease of surface functionalization, regeneration and reusability.[20,21] These characteristics make them ideal adsorbent materials for the removal of various contaminants from wastewater and water.[22,23] Chiral mesoporous silica has been used by different researchers as an effective adsorbent for the removal of various chiral contaminants from water.[24] Sawicki and Mercier[25] investigated cyclodextrin-modified silica for the removal of various pesticides. It was observed that the adsorption capacity of cyclodextrin-modified silica was higher than that of bare silica, owing to the creation of additional binding sites on the surface of silica after chemical functionalization. Compared to non-chiral adsorbents very limited studies have reported the synthesis of chiral adsorbents based on mesoporous silica. Therefore, it is neccessary to develop highly selective and efficient silica-based chiral adsorbents for the removal of chiral pesticides from water and wastewater.

In this study, mesoporous silica nanoparticles (MSNPs) with uniform particle size distribution were prepared using a sol–gel method. Surface functionalization of MSNPs was carried out using cellulose-based chiral selector, and an efficient chiral adsorbent for the removal of sulfoxaflor pesticide from water was prepared. The developed adsorbent was characterized by TEM, SEM, elemental analysis, FTIR spectroscopy, XRD analysis, BET analysis and BJH analysis. The effects of concentration and adsorbent dose were investigated. The experimental data for sulfoxaflor removal were analyzed using various isotherm and kinetics models. Furthermore, the used adsorbent was regenerated and re-used several times for the adsorptive removal of sulfoxaflor, and notably, the removal efficiency declined only 10% after recycling and reusing for twenty times.

2. Materials and methods

2.1 Chemicals

Tetramethyl orthosilicate (TMOS), polyethylene glycol, urea, acetic acid, sulfoxaflor (98.9%), HCl (37%), NaOH (99%), ethanol (99.8%), methanol (99.7%), and octadecyl dimethyl chlorosilane were bought from Sigma Aldrich, USA.

2.2 Synthesis of MSNPs

MSNPs were prepared according to a method reported by Chen *et al.*[26] with some modifications. Ammonium hydroxide (6.7 mL) and deionized water (5.1 mL) were mixed with absolute ethanol (70 mL), and the mixture was stirred for 20 min at room temperature. Then, tetraethyl orthosilicate (TEOS) (4 mL) was added into the mixture dropwise and stirred for 40 min at room temperature. After 40 min, the mixture was heated to 55 °C for 30 min, followed by the addition of 0.64 mL water and 4 mL TEOS. The addition of water and TEOS was repeated three times at regular intervals of 40 min. The silica particles were separated from the liquid phase by centrifugation at 3500 rpm, washed with ethanol and water and dried in an oven at 70 °C for 12 h. After drying, the silica particles were calcined at 550 °C in a muffle furnace to remove the organics and increase the pore size.

2.3 Surface modification of MSNPs

Cellulose powder (2 g) was dispersed in tetrahydrofuran (100 mL) and stirred for 20 min at room temperature. Then, 5 mL chloroacetic acid and 1 mL trimethyl amine were added into it, and the contents were heated to 80 °C for 5 h with continuous stirring to obtain product (**2**). Product (**2**) was dispersed in 100 mL THF and allowed to react with 5 mL dimethyl acetamide and 10 mL 3-aminopropyl trimethoxy silane (APTMS) at 80 °C for 5 h to obtain product (**3**). Product (**3**) was then reacted with methyl isocyanate to get product (**4**). Finally, MSNPs (3 g) were dispersed in 100 mL toluene, and 20 mg of product (**4**) was added to it through a dropping funnel with constant stirring at 100 °C under reflux for 8 h to get product (**5**). Product (**5**) was then washed thoroughly with methanol, filtered and dried in an oven at 70 °C for 10 h. The reaction scheme for the synthesis of chiral adsorbent based on MSNPs is shown in Fig. 1.

2.3 Characterization and evaluation of the developed adsorbent

The adsorbent was characterized using several characterization techniques, including elemental analysis, particle size distribution, BET analysis, BJH analysis, SEM, XRD, and FTIR spectroscopy. An NA-1500 analyzer (Carlo-Erba) was used for elemental analysis, a DLS-7000 analyzer (Otsuka, Japan) was used for particle size analysis and BELSORP-Max (Japan) was used for BET surface area analysis. An S-4200 FE-SEM (HITACHI, Japan) was used to obtain SEM images of the adsorbent, and an FT-IR spectrometer (Shimadzu Japan) was used to examine the functional groups. The concentration of sulfoxaflor after adsorption was determined using a UV-visible spectrophotometer (Agilent-4853, CA, USA). The chiral resolution capability of the adsorbent was determined by testing its selectivity for mandelic acid (MA) enantiomers. MA was used as a model solute to evaluate the chirality of the developed adsorbent by conducting dynamic and static adsorption experiments.[27] In a typical experiment, 100 mg of absorbent was added to 200 mL of aqueous R-MA and S-MA solutions (0.5 mg mL^{-1}) in conical flasks to assess the kinetic adsorption curve. A
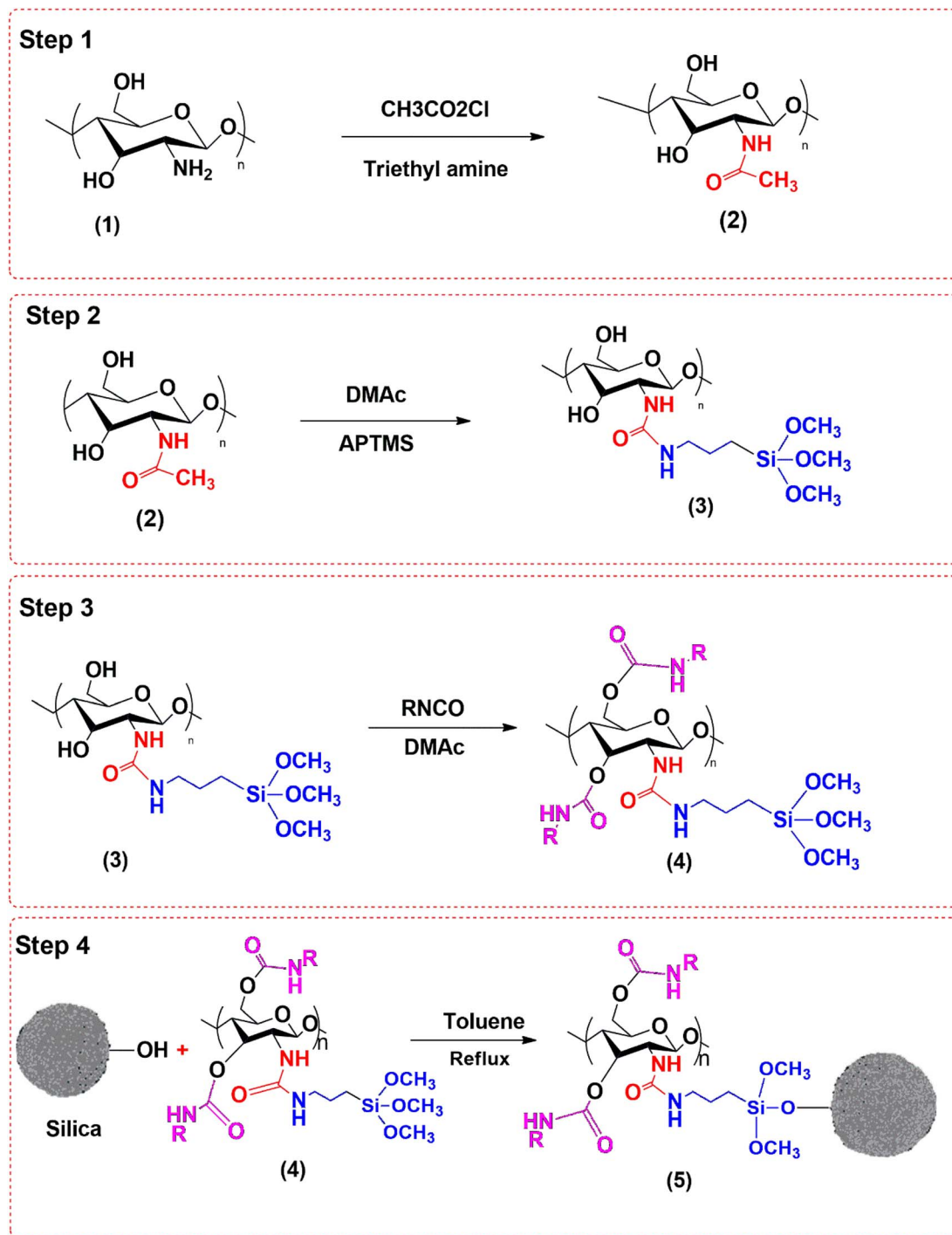
Fig. 1 Reaction scheme for the synthesis of the chiral adsorbent based on MSNPs.

magnetic stirrer was used to stir the suspension, which was incubated at 20, 30, and 40 °C. 1 mL of the sample was taken at regular intervals and centrifuged, and the MA concentration (C_t, mg mL^{-1}) in the supernatant was measured using HPLC. HPLC (LC-10AT, 15 μL injection loop, SPD-M20A detector, Shimadzu, Japan) equipped with a chiral column OD-H (150 mm × 2.1 mm) was used to examine the enantiomers of MA in various samples at 230 nm, 25 °C, and a flow rate of 0.2 mL min^{-1}. The

mobile phase was a 90 : 10 (v/v) mixture of methanol and *n*-hexane with 0.1% TFA. Prior to injection, both the samples and mobile phases were passed through a 0.45 μm membrane filter. Eqn (2) was used to determine the adsorption quantities (q, mg g^{-1}) of MA on the adsorbents. Adsorption dynamics and elution studies were used to assess the dynamic characteristics of the adsorbent for MA. A glass column (10 mm ID) was filled with 1.0 g of absorbent,[27] and the racemic MA solution (0.5 mg mL^{-1})

was passed slowly through the column at a rate of 3 BV h^{-1}. To construct the dynamic adsorption curve and determine the saturation adsorption amounts, the effluents with a single bed volume were taken and examined. Lastly, HCl solution (10%, v/v) was used as the eluting agent with a flow rate of 0.5 BV h^{-1}. The elution ratio was calculated by collecting and analyzing the eluent. The enantiomeric excess (ee%) of MA at a flow rate of 0.5 BV h^{-1} was calculated using eqn (1).

$$ee(\%) = \frac{[S] - [R]}{[S] + [R]} \times 100 \qquad (1)$$

where [S] and [R] are the concentrations of S-MA and R-MA, respectively, in the solution.

2.4. Adsorption of sulfoxaflor

The adsorption of sulfoxaflor onto functionalized MSMPs was examined through batch adsorption tests, and the optimum values of factors, such as concentration, dose, pH and time, taken for sulfoxaflor adsorption were determined. In a typical experiment, 100 mL sulfoxaflor solution of specific concentration (10–100 ppm) was added to a flask containing 0.1 g of adsorbent, and the flasks were shaken for 3 h at 40 °C in a water bath. After 3 h, the solution was filtered, and the concentration of sulfoxaflor in the filtrate was measured. The percentage removal efficiency (% R) of sulfoxaflor and the adsorption capacity (q) were calculated using eqn (2) and (3), respectively.

$$q_e = \frac{(C_0 - C_e)V}{m} \qquad (2)$$

$$\text{Removal}(\%) = \frac{(C_0 - C_e)}{C_0} \qquad (3)$$

where "m" is the adsorbent's mass (g), "V" is the solution volume in liters, "q_e" is the adsorption capacity, and C_0 and C_e are the sulfoxaflor concentrations before and after adsorption, respectively.

2.7 Adsorption isotherm and kinetic study

To find out the mechanism for the solute transfer from the aqueous phase to the adsorbent, it was necessary to analyze the experimental data with different isotherm models. The obtained numerical data on the effect of concentration of sulfoxaflor on adsorption capacity at a constant temperature was analyzed using the Freundlich and Langmuir isotherm models to elucidate the model that perfectly fits with the experimental data. Kinetic study was conducted to determine the rate at which the adsorbate molecules transfer from the solution to the adsorbent surface and the duration for which the adsorbate molecules remain on the adsorbent surface. For the kinetic study, the adsorption capacity of the adsorbent for sulfoxaflor removal was recorded by carrying out adsorption experiments at different time intervals, while concentration, dose, and pH were kept constant. Origin Pro-8 software was used for linear regression analysis and data computation. The experimental data of sulfoxaflor adsorption were analyzed using the pseudo 1st order, pseudo 2nd order, and IPD models.

2.8 Regeneration and re-use of the spent adsorbent

Adsorbent regeneration was necessary to determine the economic viability as well as the operational cost of this remediation strategy. The used adsorbent was collected and treated with various desorbing solutions, such as HCl, acetic acid, NaOH and distilled water, separately. Specific amount of the spent adsorbent was dispersed into each solution and agitated at 40 °C with an agitation speed of 100 rpm for 3 h. After 3 h, the adsorbent was rinsed three times in deionized water to ensure the removal of any contaminants and dried in an oven for re-use. The same procedure was applied for the regeneration of the spent adsorbent using HCl and distilled water.

3 Results and discussion

3.1 Characterization

3.1.1 Particle size analysis. Uniform particle size distribution is observed when most of the particles exist within the same size range. The particle size distribution of MSNPs and functionalized MSNPs are shown in Fig. 2(A). These results show that the average particle size of MSNPs is 80 nm and that of the functionalized MSNPs is around 100 nm. The results show an increase in particle size after coating with silica and functionalization as shown in Table 1(A). The polydispersity index (PdI) value of MSNPs is 0.13, which indicates that the particles are monodispersed. When the PdI value is near zero, the particle size distribution is homogeneous. Generally, if the PdI value is less than 0.3, the particles are considered monodispersed, and if it is larger than 0.5, the particles are considered heterogeneous.[28] Notably, the results of this study are
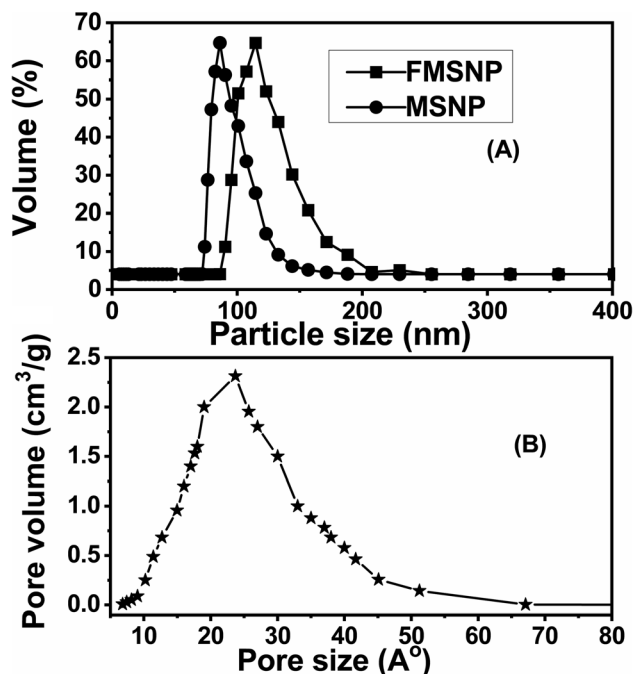

Fig. 2 Particle size distribution curve of MSNPs and functionalized MSNPs (A) and pore size distribution curve of functionalized MSNPs (B).

Table 1 Particle size (A) and pore size (B) distributions of MSNPs and functionalized MSNPs

(A) Particle size distribution	
MSNPs	Functionalized MSNPs
80 nm	100 nm

(B) Pore size distribution	
Pore diameter	23 Å
Surface area	143 m^2 g^{-1}
Average pore volume	1.74 cm^3 g^{-1}
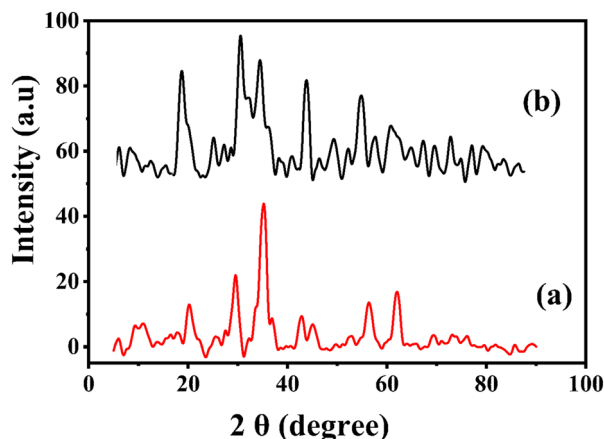
Fig. 3 X-ray diffraction analysis of functionalized MSNPs (a) and MSNPs (b).

comparable to those of a previous study reported in the literature.[29]

3.1.2 Pore size distribution. The pore size distribution of functionalized MSNPs is shown in Fig. 2(B), and the respective numerical values are presented in Table 1(B). The average pore size of the functionalized MSNPs is 23 Å, and the surface area and pore volume are 143 m^2 g^{-1} and 1.74 cm^3 g^{-1}, respectively, as shown in Table 1(B). Notably, these results align well with those of silica coated iron oxide nanoparticles reported in the literature.[30]

3.1.3 XRD analysis. XRD spectra of the functionalized MSNPs and bare MSNPs are shown in Fig. 3(a) and (b), respectively. The XRD spectrum of MSNPs (Fig. 3b) exhibits several peaks at $2\theta = 20°–35°$, which indicates there are no impurities in the silica nanoparticles prepared using the sol–gel method. On the other hand, the XRD spectrum of functionalized MSNPs shows several peaks at 2θ ranges of 29.20°, 37.02°, 58.53° and 62.53°.[30] Interestingly, a similar XRD pattern was observed by other researchers for mesoporous silica particles.[29,31,32]

3.1.4 Morphology. SEM and TEM images of bare and functionalized MSNPs are shown in Fig. 4. The SEM images show the textural features of the particles, while the TEM images provide detailed information of the particles, such as porosity and ligand chains on the surface. The SEM image of bare MSNPs in Fig. 4(A) shows that the particles are homogenous and well distributed without any agglomeration. Similarly, the TEM image of single bare MSNP particles in Fig. 4(C) shows the porous structure of the silica particles. The SEM image of a single functionalized MSNP shows a highly porous structure, as presented in Fig. 4(B), while the corresponding TEM image shows the growth of ligands over the particle surface, as shown in Fig. 4(D).

3.1.5 FTIR analysis. The FTIR spectra of bare MSNPs, synthesized polymer and functionalized MSNPs are shown in Fig. 5. The FTIR spectrum of bare MSNPs shows two prominent peaks at 3410 cm^{-1} and 1060 cm^{-1}, which correspond to the OH stretching vibration of surface silanol and the asymmetric stretching vibration of Si–O–Si, respectively.[32] The FTIR spectrum of the synthesized polymer is shown in Fig. 5(b). The bands at 3310 cm^{-1}, 2950 cm^{-1}, and 2870 cm^{-1} represent N–H stretching, aliphatic C–H stretching, and –OCH$_3$ stretching, respectively. Similarly, the bands at 1690 cm^{-1} and 1440 cm^{-1} represent C=O stretching and OH bending vibration frequencies, respectively. The FTIR spectrum of functionalized MSNPs is shown in Fig. 5(c). The peak at 3470 cm^{-1} represents the amide group.[33] The peak intensity in the OH stretching region is not as prominent as in bare MSNPs, which indicates that most of the silanol groups are functionalized with the polymer. Similarly, the bands at 1710 cm^{-1} and 1440 cm^{-1} represent C=O stretching and OH bending vibration frequencies, respectively, which is also present in the FTIR spectrum of the synthesized polymer. Thus, the FTIR results confirmed that the polymer was successfully grafted onto the surface of MSNPs.

3.2 Effect of parameters on sulfoxaflor removal

3.2.1 Effect of concentration. The effect of concentration on sulfoxaflor removal was evaluated by varying the solution concentration during batch adsorption experiments while keeping other parameters such as dose, time and pH constant. The effect of concentration on sulfoxaflor removal by functionalized MSNPs is shown in Fig. 6(a). Sulfoxaflor solutions of different concentrations (20, 40, 60, 80, 100 ppm) were tested at pH 6, temperature 40 °C, time 90 min, agitation speed of 300 rpm and an adsorbent dose 10 mg L^{-1}. It was noted that % R was low at low concentrations and gradually increased until reaching the optimum concentration of 60 ppm. At the optimum concentration, the % R reached the maximum value of 98.5 ± 0.707%. However, increasing the concentration beyond the optimum value decreased the % R, as at higher concentrations, the interactions between the adsorbate molecules increases and their interaction with the adsorbent surface decreases.

3.2.2 Effect of adsorbent dose. The relationship between adsorbent dose and % R of sulfoxaflor is shown in Fig. 6(b). This effect was studied by varying the amount (2, 6, 10, 15, 20 mg L^{-1}) of functionalized MSNPs at a constant pH value of 6 and an initial concentration of 100 ppm, followed by equilibration for 90 min at 40 °C. Results show that at low adsorbent doses (2–10
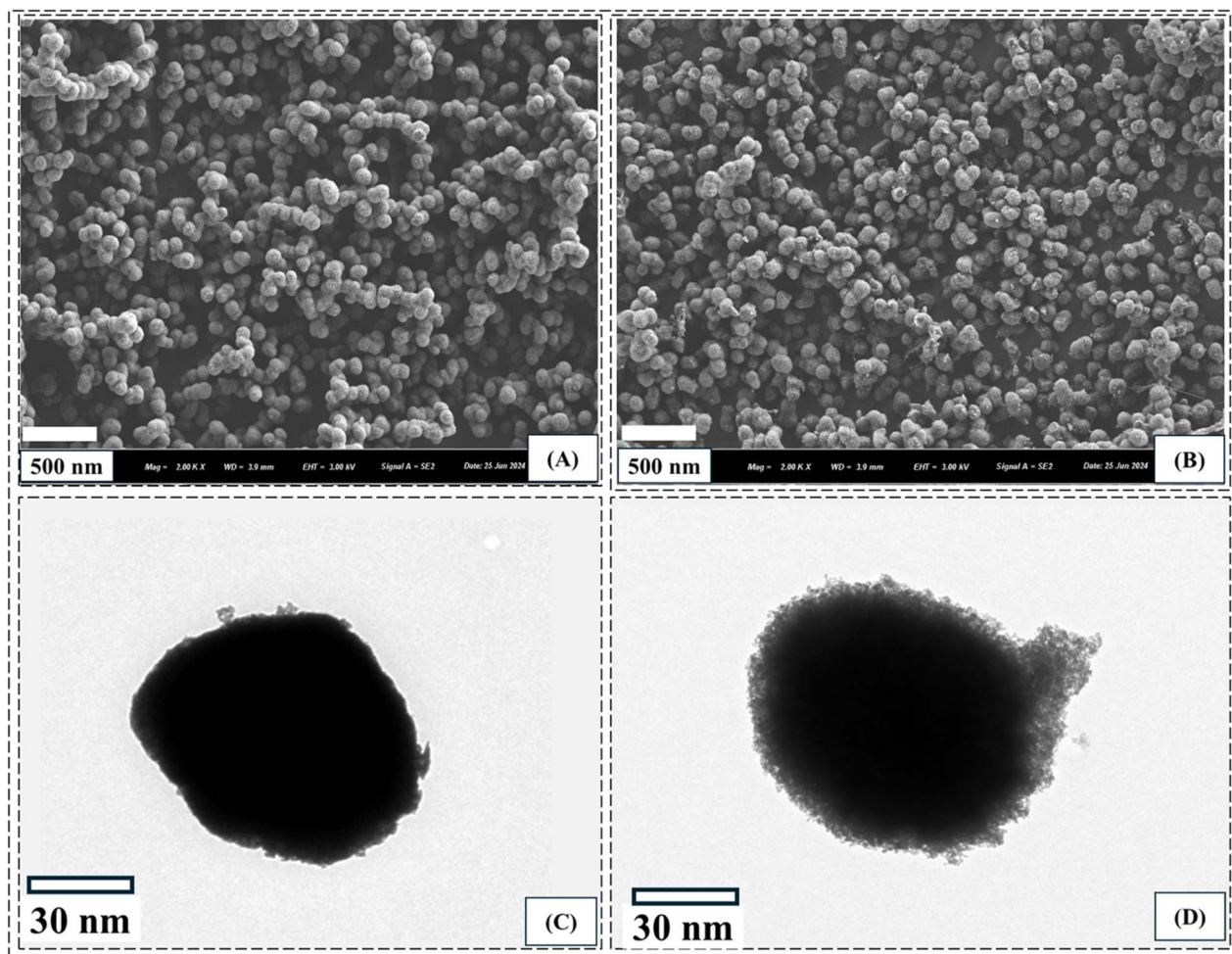
Fig. 4 SEM images of MSNPs (A) and functionalized MSNPs (B) and TEM images of MSNPs (C) and functionalized MSNPs (D).

mg), the % R increased from 80% to 98.4% for functionalized MSNPs owing to an increase in the available active sites for adsorbate molecules. Beyond this optimum value (10 mg), further increase in the adsorbent dose did not affect the % R

Fig. 5 FTIR spectra of SiO$_2$ NPs (a), synthesized polymer (b) and SiO$_2$ functionalized with the polymer (c).

value, and the removal efficiency was stabilized around 98 ± 0.579%.

3.2.4 Effect of pH. Sulfoxaflor solutions were examined by varying the pH (2, 4, 6, 8, 10) and keeping other factors constant. The solutions were placed in a water bath for 90 min at 40 °C while keeping the concentration of sulfoxaflor at 100 ppm and adsorbent dose at 10 mg L^{-1}. The results in Fig. 6(c) show that % R of 98% was obtained at pH 6 for sulfoxaflor. At low pH, the sulfoxaflor adsorption was low because of the increased H$^+$ concentration. These H$^+$ ions interacted with negatively charged adsorbent and hindered the interaction between the adsorbent and the sulfoxaflor molecules. However, the % R of sulfoxaflor increased when the pH was raised and reached its maximum at pH 6. Further elevation in pH decreased the % R of sulfoxaflor and reached the minimum value of 74 ± 0.832% at pH 10. At a high pH, the hydroxyl ion concentration increased, which further reduced the sulfoxaflor adsorption.

3.2.3 Effect of time. The effect of adsorption time on % R of sulfoxaflor is shown in Fig. 6(d). The adsorption of sulfoxaflor was carried out for 30–150 min, and the results show that during 30–90 min, the removal efficiency increased and reached the maximum value of 98.5 ± 0.883% at 90 min. After 90 min,
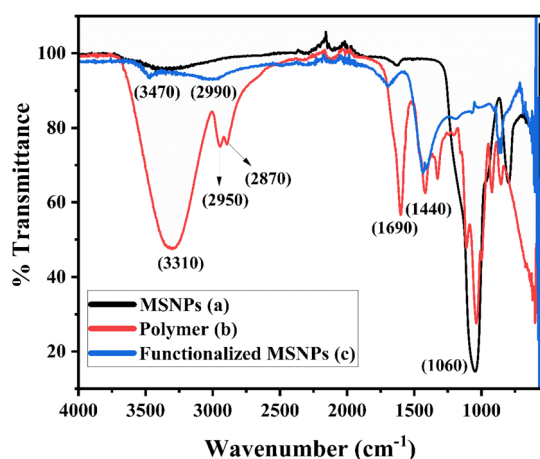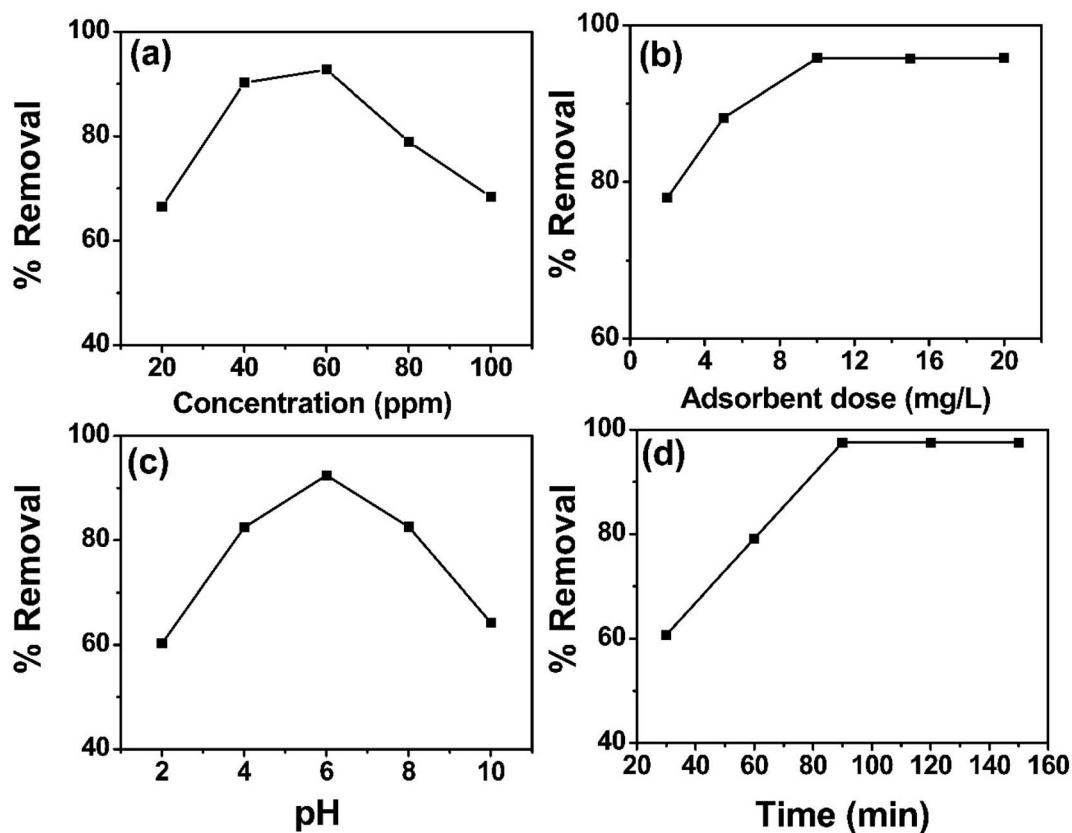
Fig. 6 Effect of concentration (a), adsorbent dose (b), pH (c) and contact time (d) on sulfoxaflor using functionalized MSNPs.
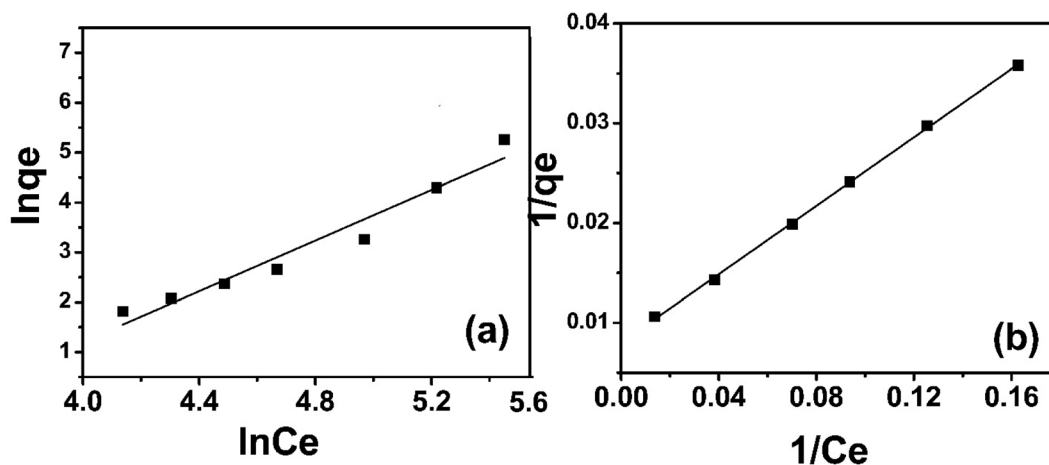

Fig. 7 Freundlich adsorption isotherm (a) and Langmuir adsorption isotherm (b) for sulfoxaflor removal using functionalized MSNPs.

the % R remained constant. The significant rise until 90 min was due to the longer interaction time between sulfoxaflor molecules and the adsorbent. Further increase in contact time showed no effect on sulfoxaflor adsorption as the active sites were saturated.

3.3 Adsorption isotherm study

3.3.1 Freundlich isotherm. The linear form of Freundlich adsorption model is presented in eqn (4).

$$\ln q_e = \ln K + \frac{1}{n}\ln C_e \tag{4}$$

The experimental data of sulfoxaflor adsorption onto functionalized MSNPs were plotted on the Freundlich isotherm model, and the plots are shown in Fig. 7(a). By plotting ($\ln q_e$) vs. ($\ln C_e$), linear plots were obtained. The "n" values are greater than zero, indicating the effectiveness of the adsorbent. The experimental data of sulfoxaflor adsorption onto functionalized

Table 2 Adsorption isotherm parameters for the Freundlich and Langmuir isotherm models

Adsorbent	Freundlich model			Langmuir model		
	$1/n$	K_F (mg g^{-1})	R^2	q_{max} (mg g^{-1})	K (L mg^{-1})	R^2
Functionalized MSNPs	0.42	52.36	0.941	435.45	60.24	0.993

MSNPs exhibited an R^2 value of 0.941, which shows that the data do not fit perfectly with the Freundlich isotherm model (Fig. 7a). Similar results for fitting experimental results of sulfoxaflor adsorption were obtained by other researchers as well.[34] Linear plots were obtained, showing logarithmic curves plotted as $\ln q_e$ *vs.* $\ln C_e$ with a slope of $1/n$. The numerical values of Freundlich isotherm constants are presented in Table 2. The results in Table 2 show that the "$1/n$" value for sulfoxaflor removal is 0.42, and the value of Freundlich constant (K_F) is 52.36 for functionalzied MSNPs.

3.3.2 Langmuir isotherm. Langmuir isotherm can be presented in mathematical form as given in eqn (5)

$$\frac{C_e}{q} = \frac{1}{q_{max}K} + \frac{C_e}{q_{max}} \quad (5)$$

where "C_e" is the equilibrium concentration of sulfoxaflor and "q_{max}" is the adsorption capacity.[35] The experimental data of sulfoxaflor adsorption onto functionalized MSNPs were plotted

using the Langmuir isotherm model, as shown in Fig. 7(b). The results in Fig. 7(b) show that the experimental data of sulfoxaflor adsorption onto functionalized MSNPs fit well with Langmuir model with an R^2 value of 0.993. The numerical values of the Langmuir adsorption isotherm for sulfoxaflor are given in Table 2. The results show that the q_{max} value for functionalized MSNPs for sulfoxaflor is 435.45 mg g^{-1}, and the K value is 60.24 (Table 2).

3.4 Adsorption kinetics

To determine the rate-determining step of sulfoxaflor adsorption onto functionalized MSNPs, batch adsorption tests were performed for different times. It was observed that until 60 min, the adsorption of sulfoxaflor onto MSNPs was fast, and at equilibrium, it slowed down. The data collected for different time intervals were computed using the pseudo 1st order, pseudo 2nd order and IPD models. The results show that the
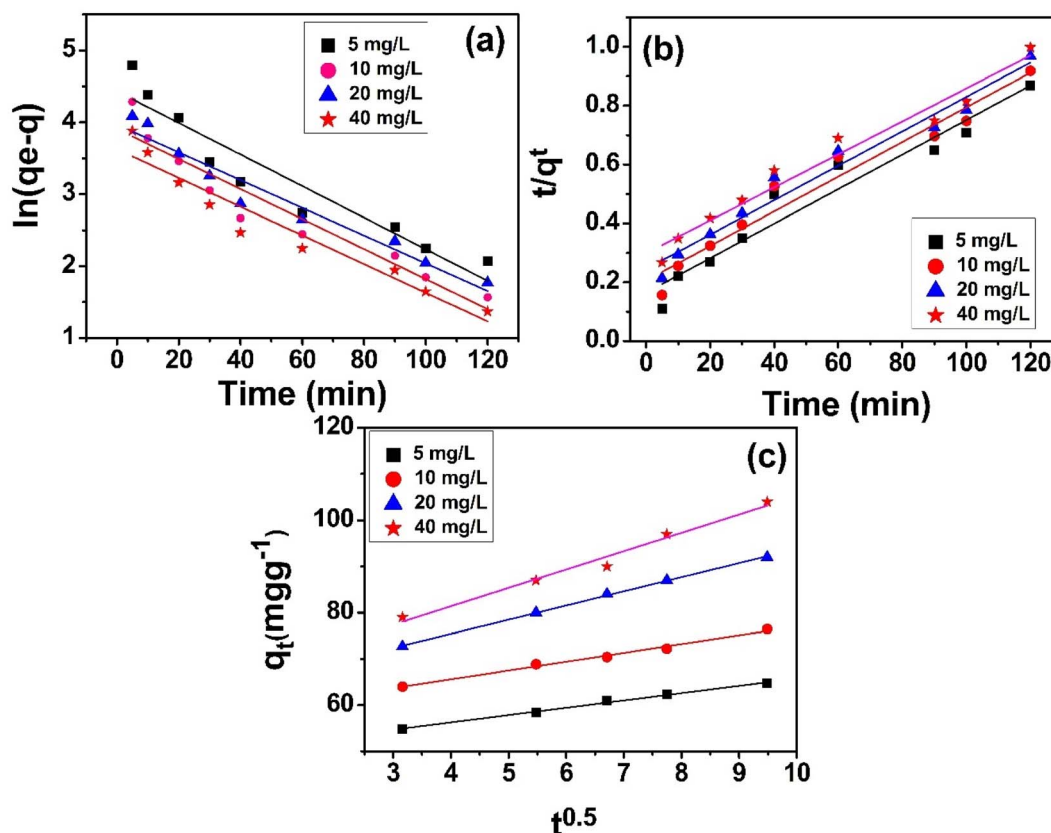

Fig. 8 Pseudo first order (a), pseudo second order (b) and intra-particle diffusion (c) model plots for sulfoxaflor adsorption onto functionalized MSNPs.

Table 3 Numerical values of pseudo 1st order, pseudo 2nd order and IPD for sulfoxaflor adsorption onto functionalized MSNPs

C_0 (mg L^{-1})		Pseudo 1st order experimental		Pseudo 1st order calculated		Pseudo 2nd order calculated		IDP calculated	
q_e (mg g^{-1})		K_1	q_e	R^2	q_e (mg g^{-1})	K_2	R^2	R^2	K_i (mg g^{-1} min^{-1})
10	132.40	0.0398	173.67	0.9693	185.34	0.0589	0.996	0.9432	4.23
20	240.72	0.0398	296.56	0.9526	298.56	0.0587	0.993	0.9521	3.50
30	387.60	0.0536	394.34	0.9678	388.75	0.0520	0.991	0.9554	4.79
40	473.22	0.0578	495.21	0.9698	485.20	0.0467	0.985	0.9620	4.94

adsorption of sulfoxaflor onto MSNPs followed the pseudo second order model.

3.4.1 Pseudo first-order kinetic model. The linear form of pseudo 1st order model is given in eqn (6).

$$\ln(q_e - q_t) = \ln q_e - k_1 t \qquad (6)$$

where k_1 represents the rate constant per minute, "q_e" is the quantity of sulfoxaflor adsorbed (mg g^{-1}) at equilibrium, and "q_t" is the quantity of sulfoxaflor adsorbed (mg g^{-1}) at a specified time (t).[34] Fig. 8(a) shows the plot $\ln(q_e - q_t)$ vs. (t) at different concentrations. The graph displays straight lines, and the slope of these plots was used for the calculation of k_1 (min^{-1}). The computed and experimental values of q_e (mg g^{-1}), R^2, K_1, and K_i (mg g^{-1} min^{-1}) for the sulfoxaflor adsorption onto functionalized MSNPs are shown in Table 3.

3.4.2 Pseudo second-order kinetic model. The pseudo 2nd order model is given in eqn (7),

$$\frac{t}{q_t} = \frac{1}{K_2 q_e^2} + \frac{t}{q_e} \qquad (7)$$

where K_2 (g mg^{-1} min^{-1}) is the constant and q_e and q_t are the concentrations of sulfoxaflor adsorbed onto functionalized MSNPs at equilibrium and at a specified time (t), respectively. The "K_2 (g mg^{-1} min^{-1})" was determined from the plot of (t) vs. (t/q_t), as shown in Fig. 8(b). The results show that the adsorption kinetics of sulfoxaflor onto functionalized MSNPs is better described by the 2nd order model.

3.4.3 Intra-particle diffusion model. The diffusion process of sulfoxaflor onto functionalized MSNPs was studied using an IPD model.[36] Eqn (8) can be used to illustrate intra-particle diffusion.

$$q_t = K_p t^{0.5} + C \qquad (8)$$

where "C" is the intercept, K_p (mg g^{-1} min$^{0.5}$) represents the IPD constant, and q_t (mg g^{-1}) is the amount of sulfoxaflor adsorbed at a specific time "t". The IPD plot of sulfoxaflor adsorption onto functionalized MSNPs is shown in Fig. 8(c). The thickness of the boundary layer is directly related to the intercept, which means that a bigger intercept value results in a larger boundary layer effect and *vice versa*.[37] As shown in Table 3, a high intercept value indicates that a thick layer of sulfoxaflor has been deposited over the adsorbent, covering the particles. Since the graphs in Fig. 8 are linear, all the three kinetic models can be applied to the adsorption of sulfoxaflor onto functionalized

MSNPs. Of these three kinetic models, pseudo 2nd order kinetic model aligns better with the experimental data for sulfoxaflor adsorption onto functionalized MSNPs.

3.5 Regeneration and reuse of the spent adsorbent

It is necessary to regenerate and reuse an adsorbent several times to assess whether the adsorption process is cost-effective.[38] Hence, the used adsorbent (4 g) was divided into four equal parts, and each part weighing 1 g was treated separately with 0.1 M HCl, 0.1 M CH$_3$COOH, 0.1 M NaOH and water. For instance, 1 g of the used adsorbent was suspended in 100 mL of the solution and shaken at 40 °C for 3 h, followed by filtration. The quantity of sulfoxaflor desorbed (%) was calculated using eqn (9).[39,40]

$$\% \text{ desorption} = \frac{\text{quantity of analyte desorbed}}{\text{quantity of analyte adsorbed}} \times 100 \qquad (9)$$

Using a variety of desorbing agents, including 0.1 M HCl, 0.1 M CH$_3$COOH, 0.1 M NaOH and distilled water, to recover and reuse the spent adsorbent, thirty regeneration cycles were conducted to assess its reusability. Fig. 9 shows the removal efficiency of regenerated adsorbent for the adsorption of sulfoxaflor and its reuse at 10, 15, 20, 25 and 30 cycles. The % R of spent adsorbent regenerated with 0.1 M HCl was the highest,
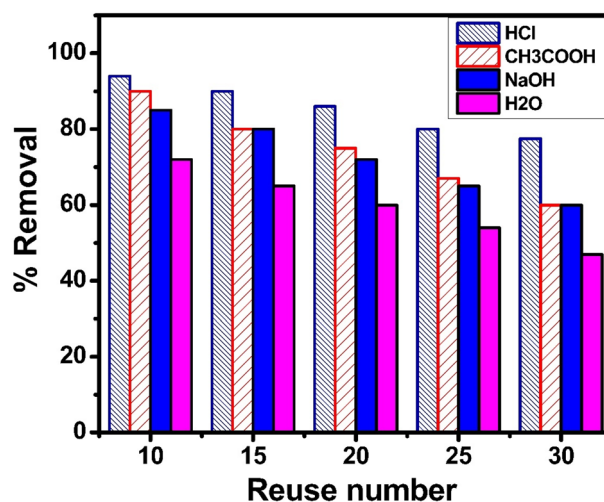

Fig. 9 Regeneration and reuse of the spent adsorbent for the removal of sulfoxaflor.

followed by 0.1 M CH$_3$COOH, 0.1 M NaOH and distilled water. These findings indicate that desorption of the adsorbate from the adsorbent surface can be achieved in an acidic medium. Moreover, the % R of the adsorbent dropped from 98.5% to 75% after thirty times of reuse, indicating that functionalized MSNPs can be used for the removal of sulfoxaflor several times after regeneration with 0.1 M HCl.

4. Conclusion

The results show that chiral MSNPs are highly effective for the removal of sulfoxaflor from water. The adsorption capacity of functionalized MSNPs was significantly higher (435.45 mg g^{-1}) owing to the highly porous nature of the silica particles and the presence of chiral functional groups. The magnetic nature of the adsorbent helped to remove it from aqueous medium using a magnet. Both the removal efficiency and adsorption capacity were reasonable. The regeneration study showed that the spent adsorbent can be regenerated and reused several times without any considerable loss in removal efficiency. Furthermore, there is scope for future studies to assess the developed adsorbent for its effectiveness in removing various other pollutants.

Data availability

The data are included in the manuscript. The raw data can be provided upon request to the corresponding author.

Author contributions

Sarah Alharthi: methodology, writing – reviewing and editing, funding acquisition, Ashraf Ali: conceptualization, writing – original draft preparation, supervision, reviewing and editing, Eman Y Santali: validation, writing – reviewing and editing.

Conflicts of interest

The authors declare no conflicts of interest.

Acknowledgements

References

1 J. R. Bertomeu-Sánchez, Introduction. Pesticides: past and present, *HoST-Journal of History of Science and Technology*, 2019, **13**(1), 1–27.

2 M. Miller and K. Bhalla, An urgent need to restrict access to pesticides based on human lethality, *PLoS Med.*, 2010, **7**(10), e1000358.

3 C. Wang, *et al.*, Enantioselectivity in estrogenic potential of chiral pesticides, *Chiral Pesticides: stereoselectivity and its Consequences*, 2011, pp. 121–134.

4 Z. Meng, *et al.*, Systematic evaluation of chiral pesticides at the enantiomeric level: A new strategy for the development of highly effective and less harmful pesticides, *Sci. Total Environ.*, 2022, **846**, 157294.

5 O. Kılıç, İ. Boz and G. A. Eryılmaz, Comparison of conventional and good agricultural practices farms: A socio-economic and technical perspective, *J. Cleaner Prod.*, 2020, **258**, 120666.

6 N. S. Sulaiman, K. Rovina and V. M. Joseph, Classification, extraction and current analytical approaches for detection of pesticides in various food products, *J. Verbraucherschutz Lebensmittelsicherh.*, 2019, **14**, 209–221.

7 F. Wang, *et al.*, Enantioselective behaviors of chiral pesticides and enantiomeric signatures in foods and the environment, *J. Agric. Food Chem.*, 2023, **71**(33), 12372–12389.

8 Y. Fang, *et al.*, Enantioselective bioaccumulation and toxicological effects of chiral neonicotinoid sulfoxaflor in rats, *Chemosphere*, 2024, **358**, 142065.

9 R. López-Cabeza and A. Francioso, Chiral pesticides with asymmetric sulfur: extraction, separation, and determination in different environmental matrices, *Separations*, 2022, **9**(2), 29.

10 A. Marican and E. F. Durán-Lara, A review on pesticide removal through different processes, *Environ. Sci. Pollut. Res.*, 2018, **25**, 2051–2064.

11 M. A. Al-Ghouti and D. A. Da'ana, Guidelines for the use and interpretation of adsorption isotherm models: A review, *J. Hazard. Mater.*, 2020, **393**, 122383.

12 Y. Wang, *et al.*, Efficient removal of acetochlor pesticide from water using magnetic activated carbon: Adsorption performance, mechanism, and regeneration exploration, *Sci. Total Environ.*, 2021, **778**, 146353.

13 J. Li, *et al.*, Metal–organic frameworks as superior adsorbents for pesticide removal from water: The cutting-edge in characterization, tailoring, and application potentials, *Coord. Chem. Rev.*, 2023, **493**, 215303.

14 Y. Dai, *et al.*, The adsorption, regeneration and engineering applications of biochar for removal organic pollutants: a review, *Chemosphere*, 2019, **223**, 12–27.

15 S. Gu, *et al.*, Clay mineral adsorbents for heavy metal removal from wastewater: a review, *Environ. Chem. Lett.*, 2019, **17**, 629–654.

16 C. De Smedt, *et al.*, Removal of pesticides from aqueous solutions by adsorption on zeolites as solid adsorbents, *Adsorpt. Sci. Technol.*, 2015, **33**(5), 457–485.

17 K. Aziz, *et al.*, Low-cost materials as vehicles for pesticides in aquatic media: a review of the current status of different biosorbents employed, optimization by RSM approach, *Environ. Sci. Pollut. Res.*, 2024, **31**(28), 39907–39944.

18 M. Brigante and M. Avena, Synthesis, characterization and application of a hexagonal mesoporous silica for pesticide removal from aqueous solution, *Microporous Mesoporous Mater.*, 2014, **191**, 1–9.

19 M. Andrunik and T. Bajda, Removal of Pesticides from Waters by Adsorption: Comparison between Synthetic Zeolites and Mesoporous Silica Materials. A Review, *Materials*, 2021, **14**(13), 3532.

20 C. Trayford and S. van Rijt, In situ modified mesoporous silica nanoparticles: synthesis, properties and theranostic applications, *Biomater. Sci.*, 2024, **12**, 5450–5467.

21 P. Das, *et al.*, Super-resolution imaging of antibody-conjugated biodegradable periodic mesoporous organosilica nanoparticles for targeted chemotherapy of prostate cancer, *Nanoscale*, 2023, **15**(28), 12008–12024.

22 A. Ali, *et al.*, Efficient removal of Pb (II) from aqueous medium using chemically modified silica monolith, *Molecules*, 2021, **26**(22), 6885.

23 X.-P. Kong, B.-H. Zhang and J. Wang, Multiple roles of mesoporous silica in safe pesticide application by nanotechnology: A review, *J. Agric. Food Chem.*, 2021, **69**(24), 6735–6754.

24 M. Cui, *et al.*, Chiral mesoporous silica materials: A review on synthetic strategies and applications, *Molecules*, 2020, **25**(17), 3899.

25 R. Sawicki and L. Mercier, Evaluation of mesoporous cyclodextrin-silica nanocomposites for the removal of pesticides from aqueous media, *Environ. Sci. Technol.*, 2006, **40**(6), 1978–1983.

26 Z. Chen, *et al.*, A non-surfactant self-templating strategy for mesoporous silica nanospheres: beyond the Stöber method, *Nanoscale*, 2020, **12**(6), 3657–3662.

27 W. Zhu, *et al.*, Fabrication and characterization of novel tentacle-type adsorbent for resolution of chiral drugs, *Chin. Sci. Bull.*, 2013, **58**, 3390–3397.

28 Y. P. Lestari and A. Amaria, Effect of ammonia-ethanol mole ratio on the silica nanoparticles synthesized for rhodamine b dyes adsorption, *J. Chem. Res.*, 2023, **8**(1), 92–104.

29 M. M. Ashour, *et al.*, Mesoporous silica nanoparticles prepared by different methods for biomedical applications: Comparative study, *IET Nanobiotechnol.*, 2021, **15**(3), 291–300.

30 Z. Gao, *et al.*, Preparation of scalable silica-coated iron oxide nanoparticles for nanowarming, *Adv. Sci.*, 2020, **7**(4), 1901624.

31 F. Tang, L. Li and D. Chen, Mesoporous silica nanoparticles: synthesis, biocompatibility and drug delivery, *Adv. Mater.*, 2012, **24**(12), 1504–1534.

32 E. Ahmadi, *et al.*, Synthesis and surface modification of mesoporous silica nanoparticles and its application as carriers for sustained drug delivery, *Drug delivery*, 2014, **21**(3), 164–172.

33 Y. Ji, *et al.*, DFT-Calculated IR Spectrum Amide I, II, and III Band Contributions of N-Methylacetamide Fine Components, *ACS Omega*, 2020, **5**(15), 8572–8578.

34 H. Abdullah, *et al.*, Bisphenol a removal by adsorption using waste biomass: isotherm and kinetic studies, *Biointerface Res. Appl. Chem.*, 2021, **11**(1), 8467–8481.

35 H. Maruyama and H. Seki, Adsorption modeling by two sites Langmuir type isotherm for adsorption of bisphenol-A and diethyl phthalate onto activated carbon in single and binary system, *Sep. Sci. Technol.*, 2022, **57**(10), 1535–1542.

36 A. Hernández-Abreu, *et al.*, Enhanced removal of the endocrine disruptor compound Bisphenol A by adsorption onto green-carbon materials. Effect of real effluents on the adsorption process, *J. Environ. Manage.*, 2020, **266**, 110604.

37 W. Li, *et al.*, Nanoplastic adsorption characteristics of bisphenol A: The roles of pH, metal ions, and suspended sediments, *Mar. Pollut. Bull.*, 2022, **178**, 113602.

38 T. Nawaz, *et al.*, Synthesis of diglycolic acid functionalized core-shell silica coated Fe_3O_4 nanomaterials for magnetic extraction of Pb (II) and Cr (VI) ions, *Sci. Rep.*, 2020, **10**(1), 10076.

39 T. Bibi, A. Ali, S. Alharthi and E. Y. Santali, Efficient removal of bisphenol A from water using C18 functionalized silica-coated iron oxide nanoparticles, *J. Nanopart. Res.*, 2025, **27**(10), 1–19.

40 A. Tayyeb, Facile synthesis of amine functionalized silica coated iron oxide nanoparticles for highly efficient removal of cefixime and ceftriaxone from wastewater, *Sep. Sci. Technol.*, 2024, **60**(2), 234–249.